NEUROSCIENCE RESEARCH NOTES

OPEN ACCESS | RESEARCH NOTES ISSN: 2576-828X

A design of an action potential generator for electrical neurons

Aiswarya K. Narayanan [1]* and Asaletha R. [2]

[1] Department of Electrical and Electronics Engineering, Cochin University College of Engineering, Cochin University of Science and Technology (CUSAT), Kochi 682022, Kerala, India.
[2] Department of Applied Science and Humanities, Cochin University College of Engineering, Cochin University of Science and Technology (CUSAT), Kochi 682022, Kerala, India.
* Correspondence: naisw4411@gmail.com; Tel.: (+91) 9497665667

Received: 26 May 2025; **Accepted**: 10 September 2025; **Published**: 23 February 2026
Edited by: Michael Ling (Universiti Putra Malaysia, Malaysia)
Reviewed by: Mohd Nazim Mohtar (Universiti Putra Malaysia, Malaysia);
Ganga Devi (Kalasalingam Institute of Technology, India);
Indranil Kushary (JIS College of Engineering, India).
https://doi.org/10.31117/neuroscirn.v9i1.475

Abstract: Recently, in the field of neuroengineering, the Action Potential Generator (APG) is an essential component used to stimulate electrical impulses during communication among neurons. Besides, the generators are required in various applications, such as neural prosthetics, brain-computer interfaces, and neuronal behavioural studies. However, traditional methods for APG in electrical neurons often rely on intricate biological systems or complex electronic circuits, which can limit efficacy and flexibility in real-time environments. In addition, these techniques can be limited in scalability, consume high power, and present issues when combined with existing neural interfaces. As a result, the proposed design creates an efficient, flexible system by combining cutting-edge materials with flexible parts. The main advancement is the combination of flexible parts and cutting-edge materials to produce a physical action potential generator with highly biomimetic and adjustable outputs. By offering previously unheard-of control and fidelity in simulating natural neural activity for research and development, particularly as a tissue-free platform for electrode testing, the generator enables a vast array of firing patterns comparable to those of biological neurons, greatly improving the reliability of neural signal transmission. Hence, the proposed APG represents a substantial advance in neuroengineering and provides a versatile and effective solution for generating electrical signals in neurons.

Keywords: Action Potential Generator (APG); Electrical neurons; Neuroengineering; Action potential; Electrical impulses.

1.0 INTRODUCTION

The field of neuroscience has progressed much in decoding the complex functioning of the brain and the neural networks (Li & Zhong, 2024). In the midst of the neuronal communication process is the action potential, a fast electrical discharge that travels along the axon of a neuron, allowing for the passage of information within the nervous system (Parveen et al.,

2024). Electrical neurons, or neurons with the major mode of communication as electrical signals, are essential in many biological phenomena such as reflex actions, sensory perception, and motor control. With advances in neuroscience, conventional techniques for recording and analyzing action potentials in electrical neurons have many limitations. Such conventional techniques rely on laborious and inexact methods, which may introduce randomness into the findings. For example, traditional electrophysiological methods, including patch-clamp recordings, are subject to being hindered by the invasive nature and inability to have stable conditions over long periods (Yousuf et al., 2025). Numerical values from these systems can differ enormously, introducing inconsistencies into data interpretation and analysis.

To meet these challenges, an Action Potential Generator (APG) for electrical neurons could provide a viable solution. Besides, the goal with the APG is to closely mimic how action potentials are naturally generated, consistently, reliably, and reproducibly (Hu et al., 2025). The value of using an APG as an experimental tool is two-fold: (i) the ability to generate action potentials in a reproducible fashion, (ii) to study and record neuronal behaviour in one particular condition while knowing that there's no variability in the experimental conditions, and (iii) further understand neuronal dynamics in health and disease. Hence, the study has proposed a design for an Action Potential Generator intended to work with electrical neurons, with improvements that could address some current constraints in existing APGs. As long as the APG is a beneficial experimental tool for basic research into neuronal function, it could lead to important developments for neurobiology, neuroengineering, and therapeutic interventions for neurological maladies (Iqbal et al, 2024).

To imitate the electrochemical dynamics of natural neurons, the APG device was created. In addition to maintaining ion concentration gradients, such as high K^+ inside and high Na^+ outside the biological cell, it will produce a synthetic membrane. Carefully regulating the "membrane's" permeability to these "mock" ions is essential for action potential generation. It is designed to react to a threshold stimulus (an electrical pulse) by rapidly increasing its "sodium" ion permeability. This depolarises the device during the rising phase of the action potential and quickly draws positive charge into it. As a result of this quick ion flux draw, "sodium" channels become inactive, and "potassium" permeability increases. This enables the device to draw positive charge out of the device, causing repolarisation and ultimately bringing the "membrane" potential back to its resting state. The shape, duration, and refractory period of a natural action potential are determined by the device's inactivation and delayed-opening mechanisms. The device is a genuinely unique tool for conducting neuroscientific research because it can fire electrically "like" a neuron by manipulating these artificial ion fluxes.

In subsequent sections, the specifics of the suggested design, with some advantages and applications in neuroscience, are provided. In addressing these issues, the APG can demonstrate how to expose the ample study of electrical neurons and contribute towards an overview of neural communication.

1.1 Neurons and action potentials

Information is transmitted throughout the body by neurons, which are the basic building blocks of the nervous system. From reflex actions to intricate cognitive processes, these specialised cells' unique ability to process and communicate signals allows for a wide range of functions. Three primary categories of neurons exist: sensory neurons, which send signals from sensory receptors to the central nervous system; motor neurons, which send signals from the central nervous system to muscles and glands; and interneurons, which link neurons in the central nervous system and are essential for information processing (Tendulkar et al., 2024). **Figure 1** illustrates the neuron's action potential.

The organisation of a neuron is finely established to serve its specific purpose. A standard neuron consists of three components: the cell body, dendrites, and a slender axon (Schneider-Mizell et al., 2025). The cell body houses the nucleus and the organelles necessary for cellular function. Dendrites are branching extensions that take in impulses from other neurons. At the same time, the axon is a long, thin projection that conveys electrical impulses from the cell body to other neurons or target tissues. Typically, the axon is covered with an insulating sheath of myelin that speeds the transmission of impulses by the process of saltatory conduction.

At the core of neuronal communication is the action potential, a rapid and transient change in the electrical membrane potential of a neuron. Action potentials are essential for the propagation of signals along the axon and are initiated when a neuron receives sufficient stimulation, leading to membrane depolarisation. This depolarisation occurs when voltage-gated sodium channels open, allowing sodium ions (Na^+) to flow into

the cell, thereby making the interior more positively charged relative to the outside. If the depolarisation reaches a certain threshold, an action potential is generated.

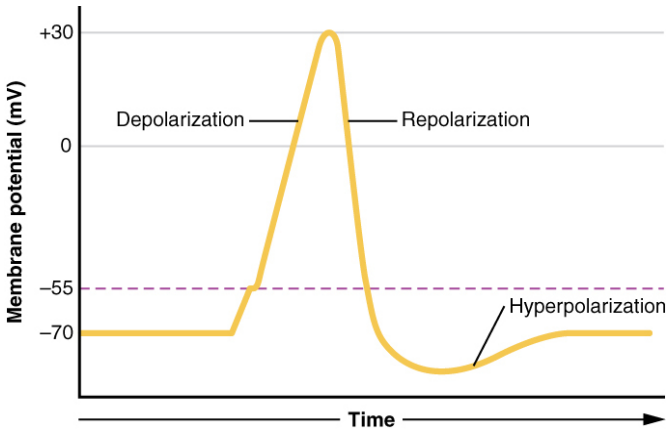

Figure 1. Illustration of neuronal action potential (Liu et al., 2025).

The action potential exhibits a distinctive chain of events. Once initial depolarisation occurs, the membrane potential increases rapidly, reaching about +30 mV (Shrivastava et al., 2024). Later on, voltage-gated potassium channels become active, allowing potassium ions (K^+) to leave the cell, repolarising the membrane to its resting potential (Palmisano et al., 2024). Then follows a temporary phase of hyperpolarisation, during which the membrane potential momentarily exceeds the resting potential, before the stable restoration of the resting potential.

The inflexible character of action potentials ensures that, after reaching the threshold, the action potential will travel down the axon without weakening. This occurs through the step-by-step opening and closing of ion channels along the axonal membrane, enabling the signal to propagate rapidly over long distances. In myelinated axons, the action potential leaps within a node of Ranvier, where the myelin sheath is missing, and there is an acceleration in its conduction (Jacak & Jacak, 2025).

The insights of action potentials are critical to fields such as neuroscience, medicine, and bioengineering. If action potential generation and propagation are impaired, this can lead to many neurological disorders, such as epilepsy, multiple sclerosis, and neuropathic pain. Thus, understanding how action potentials contribute to neuron function could inform the treatment of neurological disorders.

Hence, the neuron and action potentials are key players in the nervous system, facilitating communication and information processing (Khelfaoui et al., 2024). The physiological processes associated with action potentials are necessary for the function of neural circuitry, and the study of action potentials is an important area of study in neuroscience and allied fields.

1.2 Significance of action potential generation in neural function

Generation of the action potential is essential for optimal nervous system functioning, as it is the major method of communication between nerve cells. Through this fast electrical impulse, information can travel long distances through the body, enabling important functions such as reflexes, sensory detection, and movement coordination. The all-or-nothing nature of action potentials ensures that signals are transmitted consistently and without loss, enabling accurate control of neuronal communication. In addition, action potentials are crucial in synaptic transmission, wherein the arrival of an action potential at the axon terminal leads to the release of neurotransmitters. These chemical messengers travel across synapses to affect the activity of nearby neurons, thus mapping neural circuits and influencing behaviour, cognition, and emotional response. Interference with action potential production can result in several neurological disorders, making it crucial to maintain neural health. An understanding of the mechanisms of APG increases our insight into normal brain function but also informs the creation of therapeutic interventions for diseases such as epilepsy, multiple sclerosis, and other neurodegenerative disorders. Action potentials are therefore central to both the integrity of neural networks and the functioning of the nervous system as a whole.

1.3 Study objectives

The objectives of the research are expressed below:

- To develop a device that accurately mimics the physiological characteristics of natural action potentials in electrical neurons, by providing an unparalleled platform for the development of neurological research.
- To enhance the capacity of generating action potential by high fidelity and minimal variability, and to overcome the intrinsic limitations and

inconsistencies of conventional electrophysiological approaches.

- To provide a controlled and high-throughput platform to monitor pharmacological agents and estimate the neuronal excitability effects, and to streamline the drug discovery process for neurological conditions.
- Enable the study of action potential generation in various neurological disorders, contributing to a better understanding of disease mechanisms and potential therapeutic targets.

1.4 Literature review

This paper describes the process of creating a simple electrical circuit based on Local Activity and the Edge of Chaos Principle, combined with Circuit Theory and Nonlinear Dynamics. The circuit uses an NbOx threshold switch and is a composition requiring only one capacitor and one DC source. It produces a three-bifurcation cascade and presents a connection to a fourth-order Hodgkin-Huxley neuron model when a steady DC is applied. The construction is straightforward, uses fewer components, and demonstrates the potential of Memristors for creating energy-saving bio-inspired electronics (Ascoli et al., 2025). Recursive Piecewise Data Assimilation (RPDA) is an analytical technique for examining ionic current waveforms of hippocampal neuron recordings. RPDA successfully estimates all the ionic currents from a small, high-quality dataset. RPDA can detect alterations in non-targeted ion channels, making it useful for testing drug toxicity. The technique has been shown to accurately estimate the selectivity and potency of known ion channel inhibitors, similar to conventional pharmacological analyses (Wells et al., 2025). Neuromorphic computing systems are designed to fulfil the requirements of artificial intelligence, overcoming issues in conventional computing such as excessive power consumption and low scalability. In this paper, a neuromorphic system is proposed for digit pattern recognition with a 20x20 memristor array and an Axon-Hillock neuron model. A hard-coded approach varies the synaptic weights to identify digits from 1 to 9. The system successfully identifies these patterns, even with 5% noise interference (Choo et al., 2025).

The existing study on artificial neurons, specifically threshold switches that leverage Gas Discharge Tubes (GDTs) as prototypes, develops a Leaky Integrate and Fire (LIF) neuristor with one GDT and a more complex HH-like neuron with two GDTs, capable of expressing 24 neuronal modes. The GDTs' light sensitivity helps inhibit spiking in the LIF neuron and adjust the spiking threshold in the HH-like neuron, restoring function in photoreceptors and sensory neurons. The study has attained a miniaturisation of the GDTs and decreased their operating voltage (Trunov et al., 2025). The study presents an intelligent controller that aims to minimise seizure-like events in a memristive circuit based on the HH equations. An ANN is integrated into a Lyapunov-based control strategy to address bursting dynamics and handle uncertainties and disturbances. The effectiveness of the control strategy is rigorously established through stability analysis. Results demonstrate that the distinct controller drastically outperforms conventional nonlinear control strategies (Stiti et al., 2024). The BECI synapse circuit proposed saves area and energy and facilitates more resolution designs. It is optimized for 9 × 9-pixel images with small-bitwidth weights, resulting in reduced area and power consumption. The Spiking Neural Network (SNN) is entirely digital for comparison and includes neuron and synapse circuits. Designed using a 180 nm CMOS process, it occupies 3.6 mm² and has 94.66% accuracy on the MNIST dataset with an average power consumption of 1.06 mW, which is 20 times lower than the digital version (Dambri et al., 2025; Max et al., 2025).

The existing study defines an organic artificial neuron composed of a tiny electrochemical device. The neuron responds to liquids and to biological compounds such as dopamine and ions. It operates within real-world biological environments with specific concentration ranges and can respond to variations in ion and biomolecule concentrations. The system exhibits characteristic electrical signatures and can couple with living cell membranes to create bio-hybrid interfaces that collaborate in real time (Wang et al., 2024). This study evaluated the energy efficiency of various network topologies (BA, ER, WS networks) and the neural network of Caenorhabditis elegans. To clarify how the NN in the brain evolved with respect to energy efficiency, it applied the Hodgkin-Huxley model and energy-coding theory. The results showed that the BA network was highly energy-efficient, comparable to the neural network of C. elegans. This suggests that the brain's NN is scale-free with respect to energy efficiency. The study also linked energy consumption in neural networks with synchronization by means of energy coding (Schaufelberger, 2024). The prevailing study describes the development of neurons using a Hybrid CMOS Memristor (HCM) model, based on the Morris–Lecar (ML) design, with an innovative T-type synapse. The primary strengths of this neuron model are low power consumption in nano-watts, reduced circuit complexity, and energy efficiency in femtojoules.

The findings are the power consumption of 17. 42 pW, energy efficiency of 1.05 fJ, and a spike frequency of 28. 52 kHz (Nalliboyina & Ramachandran, 2024).

The TFET actuator LIF neuron achieved After-Hyperpolarisation (AHP) and a relative refractory period without the use of any additional hardware due to the Murray large Miller effect in combination with the forward p-i-n current that occurs in most TFET technologies. The ambipolar impact, along with the superlinear characteristics of silicon-based TFET, has also aided in developing low-cost and low-energy designs, reducing overall cost and energy consumption by nearly an order of magnitude. A Spiking Neural Network (SNN) actuator using a TFET neuron has shown great promise in various pattern recognition applications for better efficiencies (Khanday & Khanday, 2024). The study has considered whether neural spike rates consistent with the photothermal suppression technique could be maintained in a closed-loop system. Moreover, a system using gold nanorods and near-infrared light, along with a proportional-integral controller, is used. In this system, there was a feedback closed loop to reach a specific desired spike, target spike rates in cultured hippocampal neuron networks on microelectrode arrays coated with GNRs (Shabnum et al., 2025). Correspondingly, Open-loop (OL) SCS ignores changes in spacing between electrodes and the cord due to activity and posture. It results in non-uniformity in dose and tissue activation volume with each pulse. Unpredictable dosing can have an impact on treatment efficacy and duration (Kim et al., 2024). The existing study describes a chip that can simultaneously capture brain activity and stimulate the brain. The chip's design includes low-power circuits for both recording and stimulation, and consists of a means to reduce unwanted signals. Included is a closed-loop design for biomedical applications in general, and presented results from tests that utilised a chip with four recording and stimulation channels. Note that the chip was fabricated in 0.18 µm CMOS technology. Tests of the chip's ability in recording and stimulating with minimal interference of the stimulation in living organisms and animal studies verified the chip's capabilities within a successful environment (Tawade & Mastrangeli, 2024).

The raceway was a 3D printed object with four pairs of recording electrodes and two stimulation electrodes. The non-anesthetized earthworms were placed on the raceway so that their heads rested over the stimulation electrodes. The worms were subjected to different bipolar sinusoidal stimulation pulses delivered at 2 to 6 Vp-p, with pulse durations of 2 ms to 6.7 ms and a burst rate of 1 pulse per second. The study measured and analyzed the action potentials and physical movements of the worms. It was found that the action potentials corresponded to the movements of the worm segments and that the higher the stimulus voltage, the larger the action potentials that were observed. Furthermore, with multiple electrode usage, it was possible to monitor the action potential wave movement down the length of the worm in real-time (Kim et al., 2024). The existing study begins by constructing a basic neuron circuit that uses a second-order RC oscillator. Therefore, the study examines the stability and balance of the circuit under a simple neuron model. The research studies chaotic behaviours and several oscillations, such as periodic bursting and quasi-periodic spiking. It demonstrates that the circuit's stability changes throughout the bursting cycle, leading to a bifurcation that induces periodic bursting. This research has clarified the behaviour of the bifurcation and demonstrated a transition from spiking to resting. Additionally, this provides a PSIM simulation and an analogue experimental outcome with a printed circuit board confirming its conclusions (Chen et al., 2025). The study describes a type of ST production mechanism featuring a pair of special intermittent maps, which are nonlinear first-order difference equations. The first map operates with small changes at low values, then abruptly changes to a much greater value. The other map again operates with small changes at high values, then drops to a much lower value. Moreover, the ST production mechanism is capable of generating spontaneous fluctuations of membrane potential similar to actual data. It also produces spikes which have characteristic features of spikes, such as having a spike threshold in which the spike represents an energetic sharp peak, and have hyperpolarization, which is also very characteristic of biological spikes (Potirakis et al., 2025).

1.5 Problem identification

Here are certain limitations that occurred in the prevailing studies, and they are expressed below:

- The inconsistency in memristive behaviour could cause variations in synaptic strength and reliability, which could reduce the overall performance of the neuromorphic system (Schaufelberger, 2024).
- The ECAP combined with the therapy paradigms could give effective outcomes, but the challenges may occur due to the timely adjustment of stimulation parameters (Mohabbati et al., 2025).
- The sensitivity can cause inconsistent spike patterns, and it could reduce the specific dynamic conditions,

which in turn reduces the effectiveness of the application (Potirakis et al., 2025).

2.0 MATERIALS AND METHODS

2.1 Proposed action potential generation design for electrical neurons

In general, an APG in electrical neuron functionality is centred on the principles of electrochemical gradients and the ionic movements over the neuron membrane, and its working process is explained in detail.

The process starts with the maintenance of neurons at a resting membrane potential of -70 mV, due to the distribution of ions such as sodium, potassium, chloride, and calcium across the membrane, along with the sodium-potassium pump activity that actively transports sodium outside the cell and potassium inside the cell. When a neuron receives a stimulus, it induces a change in the membrane potential, and the change may be sufficient to reach the threshold level, typically near -55 mV, which triggers an action potential. When the threshold is reached, voltage-gated sodium channels open, permitting Na^+ to move towards the neuron, resulting in depolarisation as the membrane potential becomes more positive. After a certain time interval, the sodium channels close and the voltage-gated potassium channels open, causing a repolarisation as K^+ ions that flow out from the neuron and return towards the resting position. Whereas the outflow of potassium can cause hyperpolarisation at certain times, while the membrane potential is more negative than the resting potential because of the potassium channels with delayed closing. Subsequently, if the potassium channel is closed, the sodium-potassium pump helps restore the resting membrane potential by moving sodium out and potassium back into the cell. Besides, the action potential may have an inflexible response, transmitting along the axon without reducing its robustness, thereby permitting speedy communication among neurons. Hence, the process is necessary for neuronal communication and for the operation of the nervous system.

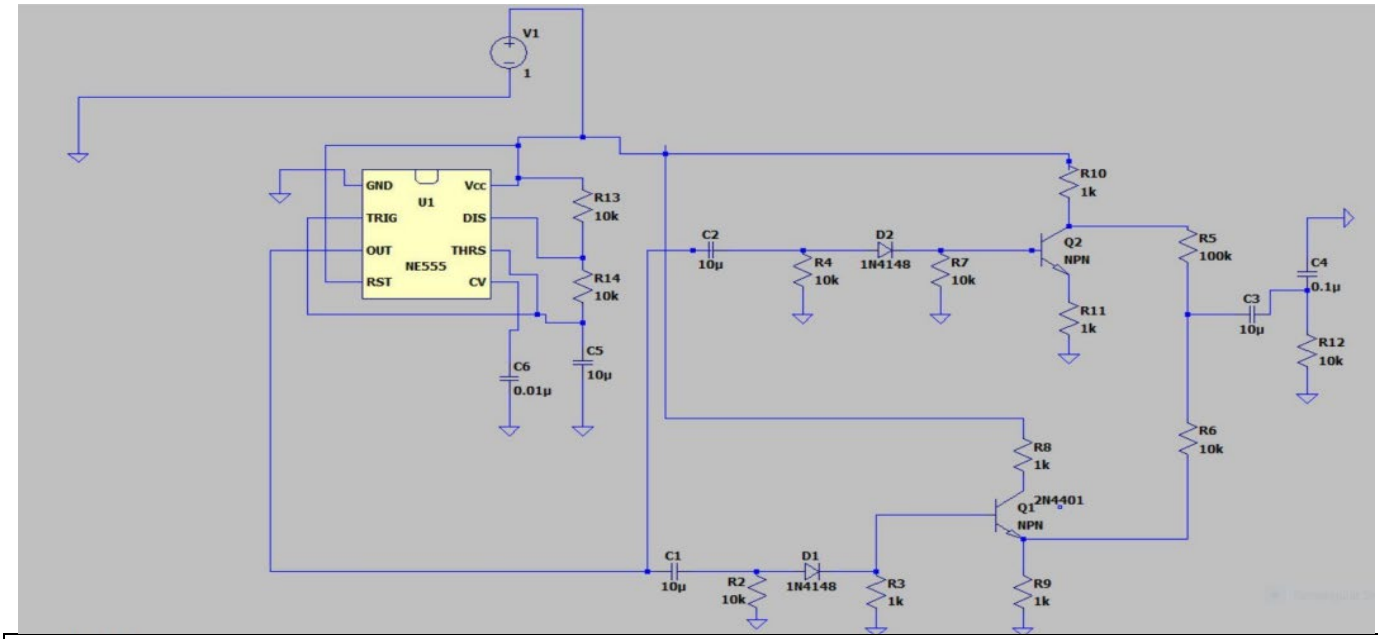

Figure 2. Design of proposed APG for electrical neurons.

Figure 2 shows the circuit that operates with two key components: a 555 timer configured as an astable multivibrator, along with the Q1 and Q2 transistor switches. Moreover, the 555 timer produces a consistent square wave, with frequencies determined by the resistors (R13, R14) and the capacitor (C5). In astable mode, the 555 timer oscillates continuously, regulating the on-off switching in the audio signal. Where the frequency (f) of the oscillation is based on the charging by R13, R14, and discharging R14 for the capacitor (C5), and it is calculated by $f = 1.44/((R13 + 2R14)C5)$, with the duty cycle of $(R13 + R14)/(R13 + 2 * R14)$. Then, the control voltage pin (CV, Pin 5) is connected to the capacitor C6 (0.01 µF) at ground, stabilizing the control voltage and reducing noise. Hence, the IC-555 timer output (Pin 3) generates a square wave and oscillates between Vcc

and ground, thereby regulating the Q1 and Q2 transistor switches.

Subsequently, Q1 acts as a switch to mute the first segment of the audio signal path. When the 555 timer output is high, current passes through C1, R2, and D1, turning on Q1. When Q1 is ON, it grounds the signal line, thereby muting the audio. When the 555 output falls low, Q1 turns off, allowing the audio signal to pass through. Component-wise, C1 acts as a coupling capacitor, isolating the DC voltage, and R2 restricts the current flowing into Q1's base. D1 (1N4148) stops reverse current flow to the 555 timer when the output is low. R3 and R9 probably act as pull-down resistors when the transistor is in the OFF state, and R8 supplies a small bias voltage to the transistor's base.

Likewise, Q2 is a switch that enables or disables the succeeding half of the audio signal pathway. Whereas, when the output of the 555 is high, the current flows through C2, R4, and D2 into Q2's base, which keeps Q2 ON and increases the audio signal's amplitude as it travels from collector to emitter. When the 555 output goes low, Q2 will turn OFF, breaking the audio signal. C2 is used as a coupling capacitor to prevent DC voltage, R4 restricts current into Q2's base, and D2 (1N4148) stops reverse current from entering the 555 timer's output when it is low. R7 limits current, and R10, R5, R11, R6, C3, C4, and R12 control the frequency response and volume of the output signal.

Therefore, the proposed circuit operates using a 555 timer in astable mode to generate a square wave. This square wave controls two transistors (Q1 and Q2), which are considered to be switches. When the switches are closed, it can turn the audio signal on and off, creating bursts of sound. The frequency of the bursts is defined by the frequency of oscillation of the 555 timer, and the components surrounding Q1 and Q2 (resistors, capacitors) determine the output quality.

The mathematical representation of the Hodgkin-Huxley (HH) model is explained and expressed below.
The membrane potential equation is provided in equation (1).

$$C_m \frac{dVm}{dt} = -(I_{Na} + I_K + I_l + I_{stm}) \quad (1)$$

Here, C_m is denoted as the membrane capacitance (µF/cm²), which accounts for the native capacity of the lipid bilayer (or its electronic equivalent in our circuit) to hold electrical charge. Increased capacitance indicates that the membrane more effectively resists voltage changes, requiring more current to achieve a certain voltage change. In our circuit design, this is equivalent to the capacitance of the "membrane" components, which determines the rate of voltage transitions.

$\frac{dVm}{dt}$ is the rate of change of membrane potential (Vm) with (t). It is the definition of the action potential – the fast depolarisation (positive dVm/dt) and the rapid repolarisation (negative dVm/dt). This measures how rapidly the voltage across the "neural" membrane shifts in response to the total current flow.

I_{Na} denotes sodium ion current, I_K is the potassium ion current, I_L signifies the leak current and I_{stm}. The stimulus current is applied externally.

I_{Na} (Sodium Ion Current): This is the entry of positively charged sodium ions into the cell. It is the major force behind the rapid depolarisation (rising phase) of the action potential. In the device, the controlled "turn-on" of a high-conductance path for "positive charge" is simulated.

I_K (Potassium Ion Current): This represents the efflux of positive potassium ions away from the cell. It is essential for the repolarisation (declining phase) of the action potential to return to the resting membrane potential. The device will mimic this by regulating a pathway for "positive charge" efflux.

I_L (Leak Current): This represents a minor, non-voltage-gated movement of ions (mainly potassium and chloride) that helps keep the resting membrane potential. In the electronic circuit, this would be similar to permanent resistive channels that establish the resting voltage.

I_{stm} (Stimulus Current): This is any current from outside the neuron that is used to drive the action potential if it is large enough to reach threshold. In our device, Istm is the trigger signal (e.g., from a 555 timer or an external source) that starts the "firing" process.

The current equation for the sodium is given below,

$$I_{Na} = gNa\, m^3\ h(V_m - E_{Na}) \quad (2)$$

Here, the maximum conductance (gNa), activation gate variable for sodium channel (m), which is a probability for activation, inactivation gate variable (h) for sodium channel, and the membrane potential (V_m) and sodium reversal potential (E_{Na}).

gNa (Peak Sodium Conductance): This is the peak possible conductance of the sodium channels when completely open. In our electronic circuit, this is the peak current rating of the "sodium" switching device (e.g., fully conducting transistor Q1).

m (Sodium Activation Gate Variable): This dimensionless probability variable (0 to 1) determines the instantaneous level of activation of the sodium channels. When the membrane depolarises (V m increases), m rapidly increases, resulting in rapid channel opening. The cubic power (m^3) indicates that three independent "m-gates" must open simultaneously for the channel to be fully conductive, resulting in a sharp, threshold-like activation.

h (Sodium Inactivation Gate Variable): This is a dimensionless probability variable (0 to 1) that regulates the inactivation of the sodium channels. Whereas m activates quickly during depolarisation, h inactivates (closes) slowly as depolarisation continues. This slow inactivation is important for restricting the duration of the sodium current, enabling repolarisation, and contributing to the absolute refractory period.

$(V_m - E_{Na})$ (Electrochemical Driving Force for Sodium): This is the "voltage difference" by which sodium ions are driven through the membrane. E_{Na} is the reversal potential for sodium, i.e., the membrane potential at which there is no net movement of sodium ions. This is the maximum voltage by which the sodium current will force the membrane.

The current equation for potassium is expressed below,

$$I_k = gK\, n^4 * (V_m - E_K) \quad (3)$$

Whereas, the maximum potassium conductance (gK), the activation gate variable (n) for the potassium channel, and the potassium reversal potential (E_K).

gK (Maximum Potassium Conductance): This is the maximum conductance possible for the potassium channels. In our device, this is equivalent to the maximum current capability of the "potassium" switching element (e.g., transistor Q2).

n (Potassium Activation Gate Variable): A dimensionless probability variable (0 to 1) that regulates the opening of the potassium gates. In contrast to m, n slowly activates upon depolarisation. The fourth power (n^4) means that four independent "n-gates" need to open, resulting in an even slower, more sigmoidal opening than with sodium, thereby coordinating repolarisation to perfection.

$(V_m - E_K)$ (Electrochemical Driving Force for Potassium): This force pushes potassium ions through the membrane. E_K is the reversal potential for potassium, the membrane potential at which there is no net movement of potassium ions. This is the fairly negative voltage to which the membrane is pushed by the potassium current, helping repolarise and even hyperpolarise.

Subsequently, the gating variable equations are depicted. The gating variables are determined using the 1st-order differential equation provided below.

$$\frac{dx}{dt} = \alpha x(V_m)\,(1 - x) - \beta x(V_m) * x$$

or (4)

$$\frac{dx}{dt} = \frac{xinf(Vm) - x}{taux(Vm)}$$

Here, x signifies the gating variables (m,h, or n), $\alpha x(V_m)$ and $\beta x(V_m)$ are the voltage-dependent rate constants for open and closed channels, $xinf(Vm)$ remains as a steady-state value of the gating variable and $taux(Vm)$ This is the time constant for the provided membrane potential.

$\alpha x(V_m)$ and $\beta x(V_m)$ (Voltage-Dependent Rate Constants): These are vital, non-linear V_m functions that control the rate of opening of the gates (αx) and closing of the gates (βx). For instance, a high $\alpha m(V_m)$ at depolarised levels guarantees fast sodium channel opening. In our digital simulation, these rates will be carefully adjusted by the individual properties of the transistors, their biasing, and the time constants introduced by nearby RC networks.

$xinf(Vm)$ (Steady-State Value): This is the steady-state value to which the gating variable x will settle if the membrane potential is maintained constant for an infinite period of time. It gives the voltage-dependent 'target' for each gate.

$\tau x(Vm)$ (Time Constant): This voltage-dependent quantity determines how rapidly the gating variable x evolves towards its steady-state value. A smaller τx implies quicker kinetics. In our circuit, these time constants are one-to-one translated to the RC values of the timing and shaping circuits that operate the

transistor switches, enabling us to strictly control the speed of "channel" activation and inactivation, thus making the generated waveform closely replicate biological action potentials.

Therefore, the APG device is designed to create the electrochemical dynamics of natural neurons. It will make a synthetic membrane that also maintains ion concentration gradients, such as high K^+ inside and high Na^+ outside the biological cell. The process of action potential generation involves carefully controlling the permeability of the "membrane" to these "mock" ions. The device is programmed to respond to a threshold stimulus (an electrical pulse) and then increase its "sodium" ion permeability extremely rapidly, rapidly drawing positive charge into the device and depolarising it - which is the rising phase of the action potential. This rapid draw of ion flux subsequently leads to the inactivation of "sodium" channels and an increase in "potassium" permeability, which allows the device to draw positive charge out, leading to repolarisation and an eventual return of the "membrane" potential to its resting state. The device is designed to provide both inactivation and delayed-opening mechanisms that shape, duration, and refractory period of a natural action potential. By controlling these artificial ion fluxes, the device can fire electrically "like" a neuron, making it a truly unique tool for neuroscientific research.

3.0 RESULTS

3.1 Performance analysis

Figure 3 shows the timing diagram for the 555 Timer output at the OUT pin, and we can also note the following. The waveform is a clean digital square wave shifting between approximately 0 V and approximately 1 V, which may represent a scaled voltage for simulation purposes. The pulse is periodic and uniform, indicating that the timer circuit is functioning correctly as an astable circuit. The waveform period is approximately 0.2 seconds, corresponding to a frequency of approximately 5 Hz.

Figure 4 depicts the measured waveform, which appears to be the output after signal conditioning and is most likely measured across C4 or R12 at the end of the circuit. The measured output shows voltage spikes in nanovolts, which most likely indicate residual noise or very weak pulses. The measured waveform has the same frequency of 5 Hz, which supports that it is still responding to the output of the 555 Timer.

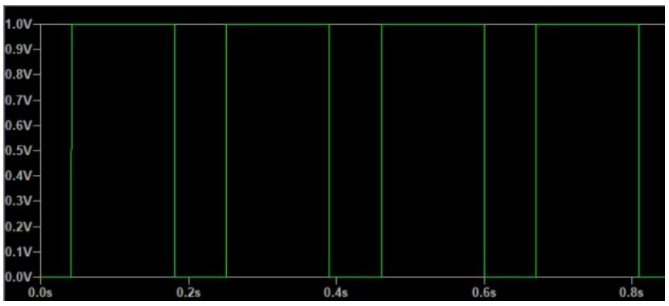

Figure 3. Illustration of input voltage (0-1 V).

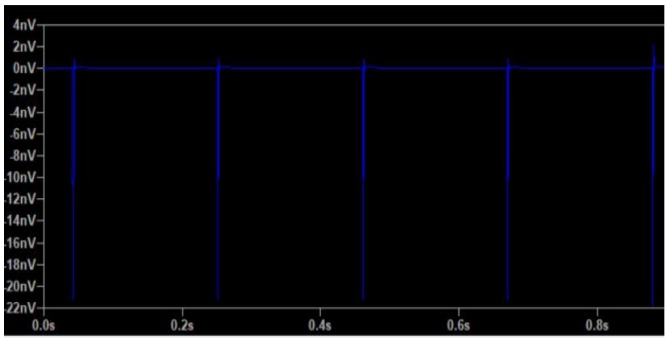

Figure 4. Outcome of output voltage (0-1 V).

The waveform indicates a very clean square wave switching between 0 V and 1.9 V (**Figure 5**). The duty cycle appears to be very close to 50%, with a period of 0.2 seconds per cycle, or roughly 5 Hz. The edges of the waveform are very clean and sharp, indicating the signal should have good rise and fall times. This output was likely produced by the transistor amplification and buffering stage of Q1 or Q2, as in the original circuit. Although faint, the output level has increased slightly from the previous 1 V output from just the 555 Timer, indicating that the transistors were able to actively drive the signal with the amplification provided by the transistors.

Figure 6 illustrates the voltage in microvolts (µV), from 10 µV to -140 µV (y-axis), and the x-axis denotes time in seconds (s), ranging from 0.0 to 0.8 seconds. The green line represents the waveform of the recorded signal. From the graph, the signal had a flat voltage just below 0 µV, visible as numerous sharp negative spikes. The high negative spikes are sudden voltage drops, with approximately equal spacing, down to about -140 µV, and then return to the same voltage level. An oscilloscope captures and displays electronic signals as they occur; it records voltage waveforms and signal-integrity measurements and helps debug circuit failures.

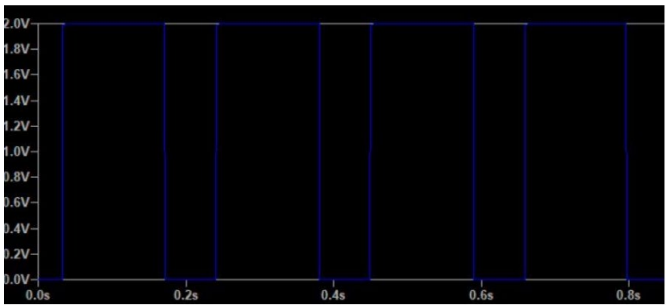

Figure 5. Representation of input voltage (0-2 V).

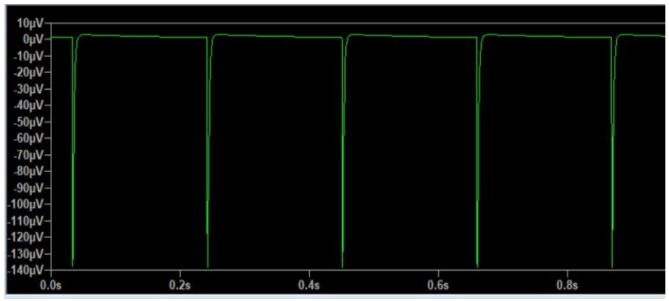

Figure 6. Obtained output voltage (0-2 V).

Figure 7 shows the waveform, which appears to be a square wave, with a roughly 2.9 V peak and oscillating down to nearly 0 V. This waveform has a greater amplitude than the previous still image. Yet the period and frequency appeared to be the same as before (approximately 5 Hz), indicating that it likely came from the same signal path, just amplified. Therefore, this signal is more powerful than the previous one, confirming that there is another amplification stage in the output, and it is closer to the pulse circuit's final output. It is likely that the transistor, perhaps Q2, is acting as a buffer or final driver stage at this output, clearly amplifying the output voltage to a level capable of triggering other devices.

Figure 8 shows that the waveform above is significantly different from the first two; it is a square wave with a sharp spike, with upper and lower limits of approximately +50 mV and -15 mV, respectively. The frequency remains unchanged from the previous two waveforms at approximately 5 Hz, so it is likely still a response of the same periodic signal. It is possible that this waveform was measured across a coupling capacitor (C3 or C4) that allows only high-frequency or transient components to flow during conduction. In this state, the spikes respond to the differentiated edge of the square wave, as the entire pulse is not depicted in the parameters of the edges of the pulse. It is also possible that this was a measurement of a sensing node or an output filtering node and would only record the degrees of the transients.

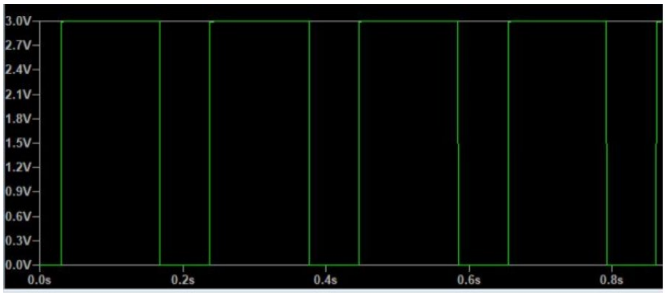

Figure 7. Input voltage (0-3 V) representation

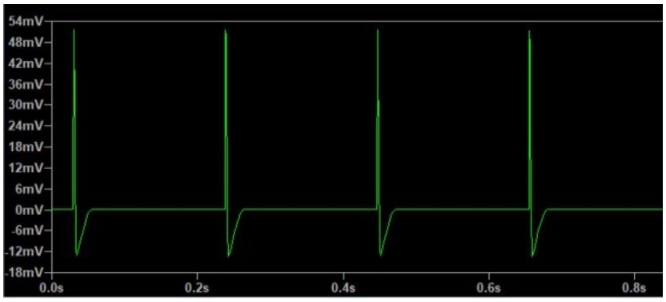

Figure 8. Obtained output voltage (0-3 V).

Figure 9 illustrates that the signal is green and the Y-axis ranges from 0 V to +4 V. The time frame is on the X-axis, ranging from 0 to 1 second. The signal completes a cycle every 0.1 to 0.2 seconds. The waveform is a pure rectangular square wave that runs from 0 to +4 volts and has a 50% duty cycle, meaning it spends the same amount of time in the high and low states. This signal is certainly a digital input or clock pulse used to drive or initiate another part of the system.

Figure 10 shows the waveform, represented in blue, which has an overall voltage that oscillates much less than the first, from -40 mV to +200 mV. The waveform has sharp transitions with peaks of approximately 180 mV, followed by a momentary excursion below 0 V. This waveform also exhibits a slight overshoot and ringing after the sharp transition, since ringing typically indicates an a/c-influenced circuit with capacitive or inductive effects. This example most likely is an output from a sensor, amplifier, or switching node somewhere because of the change in the input square wave, likely in reference to a sensed current or voltage drop across a device such as a shunt resistor. The waveform output

most likely indicates the collector voltage of a transistor or buffer responding to the square wave. The dynamics of this waveform are evident due to the shape of the waveform, as it is not a static digital output.

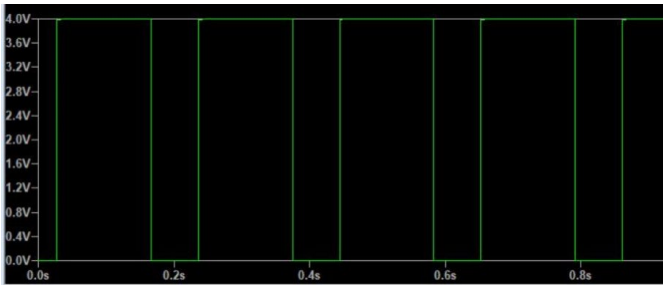

Figure 9. Input voltage (0-4 V).

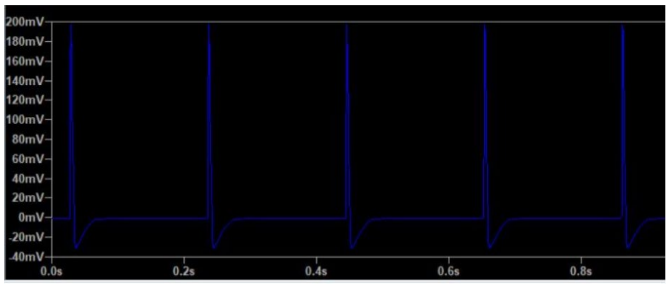

Figure 10. Outcome of output voltage (0-4 V).

Figure 11 shows that the waveform is in green and the voltage swings between 0 V and 5 V, which is typical of Transistor-Transistor Logic (TTL) or CMOS digital logic levels. It is a clean square wave, as was the first waveform, though it has slightly different voltage levels, now operating between 0 V and 5 V rather than 0 V and 4 V. This is most likely the output of a switch, whether a MOSFET or a logic gate that takes the signal from the waveform output shown above. It could also be the regulated output from a digital driver circuit.

Figure 12 shows a plot of a repeating waveform versus time. The x-axis represents time in seconds, and the y-axis is in millivolts (mV) and is a repetitive waveform that has pointed spikes followed by a flat period. It occurs about every 0.2 seconds. The waveform likely indicates that it is a pulsed or similar electrical signal.

4.0 DISCUSSION

Primarily, the existing study (Fu et al., 2025) has represented functional parameters such as the signal amplitude and the higher magnitude levels of the signals. But they do not align with the standard biological metrics. Thus, this mismatch has limited the inclusion of real-time systems, leading to disrupted power signals and lowered utilisation of in bio-hybrid circuits. Whereas the proposed design has achieved the scaled outputs precisely, which directly matches the lower potential values found in actual biological neurons. Moreover, the proposed system utilises the Bio-Amplitude signal generation method, which can be applied in bio-hybrid circuits.

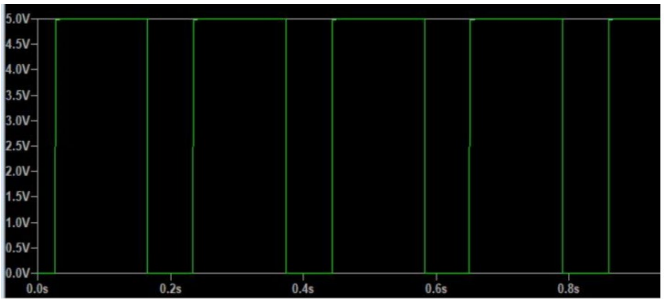

Figure 11. Input voltage (0-5 V).

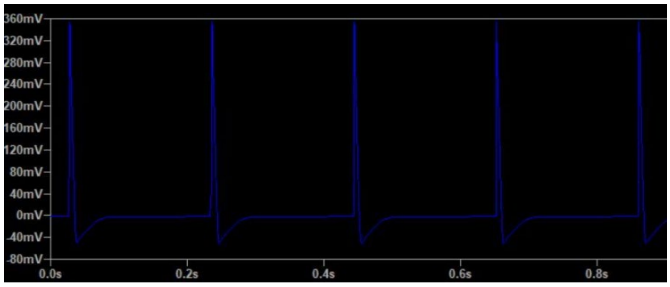

Figure 12. Outcome acquired by output voltage (0-5 V).

However, the considered study (Raj, n.d.) has stated some foremost challenges in the process of generating neurological action potentials, such as irregular, noisy, and dynamic signals. These irregularities can significantly impair the analysis of the data and may require compound designs to enhance the detected signals. In contrast, the proposed system has generated stable, uniform signals at a consistent frequency of 5Hz, ensuring low-noise output and improving data analysis of the signals.

Similarly, the existing study (Deshmukh et al., 2025) has utilised Electrically Evoked Compound Action Potential (ECAPs) to elicit neuronal responses and has stated that these ECAPs have been subjected to multiple disturbances, such as motion artefacts. These disturbances can decentralise the signal integrity by introducing variations into the generated responses,

often leading to a misconception of the actual neural signals. Whereas the proposed study demonstrated clean digital square waves and sharp edges, which shows that the proposed design can efficiently mitigate the artefacts, ensuring high signal integrity.

Furthermore, the prevailing study (Hussain et al., 2024) has demonstrated the need for accurately constructed action potential generator designs to ensure effective signal generation. The considered study has also implied that the conventional designs have suffered from inaccurate outcomes, which can be unsuited for real-time utilizations or large-scale optimisation of the biological signals. While the proposed action potential generator has produced effective outputs at standard digital logic levels, it has ensured that the proposed design is suitable for larger models.

5.0 CONCLUSIONS

The action potential as a source of electrical activity in neurons was a breakthrough in understanding how it's triggered and controlled through the circuit. By paralleling the natural process of neuronal firing, this generator provides opportunities to study neuronal behaviour that were previously unavailable and suggests distinct possibilities for therapeutic intervention in neurobiology and medicine. The TOBs featuring advanced materials and precise control are capable of generating action potentials that are highly similar to those of biological neurons, which is very helpful for studies. Furthermore, the possible uses of these technologies go beyond basic research. These technologies can play a crucial part in neuroprosthetics and provide new approaches to treatment for many individuals with neurological disorders or injuries. The formation of this action potential generator will improve many patients' quality of life by restoring lost functions. While it iterates on this version of the design, future work will seek to enhance the approach's efficiency and scalability and make it compatible with other neural interfaces. Continued collaboration between engineers, neuroscientists, and clinicians will be key to turning such advances into the clinic. Hence, the APG remains an example of the usefulness of interdisciplinary research, offering progress toward transformative discoveries that may change the way treatment is provided for neurological diseases.

Acknowledgements: None.

Author Contributions: AR conceptualised the project; AKN implemented the project and collected the data; AKN wrote the initial manuscript; AKN and AR revised and edited the manuscript.

Conflicts of Interest: The authors report no conflict of interest.

References

Ascoli, A., Demirkol, A. S., Messaris, I., Ntinas, V., Prousalis, D., Slesazeck, S., Mikolajick, T., Corinto, F., Bonnin, M., & Gilli, M. (2025). Edge of chaos theory unveils the first and simplest ever reported Hodgkin–Huxley neuristor. *Advanced Electronic Materials*, *11*(8), 2400789. https://doi.org/10.1002/aelm.202400789

Chen, B., Liu, Y., Bao, H., Zhang, X., & Bao, B. (2025). Coexisting and bursting oscillations in a second-order RC-oscillator-based piecewise linear neuron circuit. *Nonlinear Dynamics*, *113*, 17141–17159. https://doi.org/10.1007/s11071-025-11007-4

Choo, J. W., Nath, S., & Kumar, T. N. (2025). *Neuromorphic computing using memristor synapses and CMOS neurons.* Research Square. https://doi.org/10.21203/rs.3.rs-6324848/v1

Dambri, O. A., Azarnoush, A., Makrakis, D., Levesque, G., Witter, M., & Hafid, A. S. (2025). Design and implementation of a simulation framework for a bio–neural dust system. *Modelling*, *6*(1), 8. https://doi.org/10.3390/modelling6010008

Deshmukh, A., Settell, M., Cheng, K., Knudsen, B., Trevathan, J., LaLuzerne, M., Blanz, S., Skubal, A., Verma, N., & Romanauski, B. (2025). Epidural spinal cord recordings (ESRs): Sources of neural-appearing artifact in stimulation evoked compound action potentials. *Journal of Neural Engineering*, *22*(1), 016050. https://doi.org/10.1088/1741-2552/ad7f8b

Fu, S., Gao, H., Wang, S., Wang, X., Woodard, T., Wang, Z., Kong, J., Lovley, D. R., & Yao, J. (2025). Constructing artificial neurons with functional parameters comprehensively matching biological values. *Nature Communications*, *16*(1), 8599. https://doi.org/10.1038/s41467-025-63640-7

Hu, C., Yang, Q., Liu, Y., Röddiger, T., Butkow, K.-J., Ciliberto, M., Pullin, A. L., Stuchbury-Wass, J., Hassan, M., & Mascolo, C. (2025). *A survey of earable technology: Trends, tools, and the road ahead*. arXiv Preprint. https://doi.org/10.48550/arXiv.2506.05720

Hussain, M. A., Grill, W. M., & Pelot, N. A. (2024). Highly efficient modeling and optimization of neural fiber responses to electrical stimulation. *Nature Communications*, *15*(1), 7597. https://doi.org/10.1038/s41467-024-51709-8

Iqbal, M. S., Heyat, M. B. B., Parveen, S., Hayat, M. A. B., Roshanzamir, M., Alizadehsani, R., Akhtar, F., Sayeed, E., Hussain, S., & Hussein, H. S. (2024). Progress and trends in neurological disorders research based on deep learning. *Computerized Medical Imaging and Graphics*, *116*, 102400. https://doi.org/10.1016/j.compmedimag.2024.102400

Jacak, J., & Jacak, W. (2025). Ionic plasmon-polaritons in neural signaling II: Control role of the myelin over frequency and speed of stimulus in axons. *Plasmonics*, *20*, 11331–11347. https://doi.org/10.1007/s11468-025-03212-z

Khanday, M. A., & Khanday, F. A. (2024). A bio-inspired ferroelectric tunnel FET-based spiking neuron for high-speed energy efficient neuromorphic computing. *Micro and Nanostructures*, *188*, 207788. https://doi.org/10.1016/j.micrna.2024.207788

Khelfaoui, H., Ibaceta-Gonzalez, C., & Angulo, M. C. (2024). Functional myelin in cognition and neurodevelopmental disorders. *Cellular and Molecular Life Sciences*, *81*(1), 181. https://doi.org/10.1007/s00018-024-05222-2

Kim, H.-S., Baby, T., Lee, J.-H., Shin, U. S., & Kim, H.-W. (2024). Biomaterials-enabled electrical stimulation for tissue healing and regeneration. *Med-X*, *2*(1), 7. https://doi.org/10.1007/s44258-024-00020-8

Li, Y., & Zhong, Z. (2024). Decoding the application of deep learning in neuroscience: A bibliometric analysis. *Frontiers in Computational Neuroscience*, *18*, 1402689. https://doi.org/10.3389/fncom.2024.1402689

Liu, L., Yun, Z., Manubens-Gil, L., Chen, H., Xiong, F., Dong, H., Zeng, H., Hawrylycz, M., Ascoli, G. A., & Peng, H. (2025). Connectivity of single neurons classifies cell subtypes in mouse brains. *Nature Methods*, *22*(4), 861–873. https://doi.org/10.1038/s41592-025-02621-6

Max, K., Sames, L., Ye, S., Steinkühler, J., & Corradi, F. (2025). Synthetic biology meets neuromorphic computing: Towards a bio-inspired olfactory perception system. *Neuromorphic Computing and Engineering*, *5*, 034010. https://doi.org/10.1088/2634-4386/aded2d

Mohabbati, V., Sullivan, R., Yu, J., Georgius, P., Brooker, C. D., Siorek, M., McClelland, N. L., Coletti, F., Sun, X., & Franke, A. (2025). Early outcomes with a flexible ECAP based closed loop using multiplexed spinal cord stimulation waveforms—single-arm study with in-clinic randomized crossover testing. *Pain Medicine*, *26*(11), 773–782. https://doi.org/10.1093/pm/pnaf058

Nalliboyina, K., & Ramachandran, S. (2024). An energy-efficient hybrid CMOS spiking neuron circuit design with a memristive based novel T-type artificial synapse. *AEU-International Journal of Electronics and Communications*, *173*, 154982. https://doi.org/10.1016/j.aeue.2023.154982

Palmisano, V. F., Anguita-Ortiz, N., Faraji, S., & Nogueira, J. J. (2024). Voltage-gated ion channels: Structure, pharmacology and photopharmacology. *ChemPhysChem*, *25*(16), e202400162. https://doi.org/10.1002/cphc.202400162

Parveen, S., Showkat, F., Badesra, N., Dar, M. S., Maqbool, T., & Dar, M. J. (2024). Axonal degeneration, impaired axonal transport, and synaptic dysfunction in motor neuron disorder. In A. Khan, M. A. Rather & G. M. Ashraf (Eds.), *Mechanism and Genetic Susceptibility of Neurological Disorders* (pp. 199-229). Springer.

Potirakis, S. M., Diakonos, F. K., & Contoyiannis, Y. F. (2025). A Spike Train Production Mechanism Based on Intermittency Dynamics. *Entropy*, *27*(3), 267. https://doi.org/10.3390/e27030267

Raj, P. (2025). Neural networks for real-time signal processing in nano-bio-electronic devices. *International Journal of Scientific Research and Engineering Development*, *8*(3), 1332-1337. https://doi.org/10.5281/zenodo.15577848

Schaufelberger, M. (2024). *Spiking neural networks for control* [Masters thesis, KTH Royal Institute of Technology]. Publications KTH.

Schneider-Mizell, C. M., Bodor, A. L., Brittain, D., Buchanan, J., Bumbarger, D. J., Elabbady, L., Gamlin, C., Kapner, D., Kinn, S., & Mahalingam, G. (2025). Inhibitory specificity from a connectomic census of mouse visual cortex. *Nature*, *640*, 448-458. https://doi.org/10.1038/s41586-024-07780-8

Shabnum, S. S., Siranjeevi, R., Raj, C. K., Nivetha, P., & Benazir, K. (2025). A comprehensive review on recent progress in carbon nanotubes for biomedical application. *Environmental Quality Management*, *34*(3), e70040. https://doi.org/10.1002/tqem.70040

Shrivastava, A., Kumar, A., Aggarwal, L. M., Pradhan, S., Choudhary, S., Ashish, A., Kashyap, K., & Mishra, S. (2024). Evolution of bioelectric membrane potentials: Implications in cancer pathogenesis and therapeutic strategies. *The Journal of Membrane Biology*, *257*(5-6), 281–305. https://doi.org/10.1007/s00232-024-00323-2

Stiti, C., Benrabah, M., Aouaichia, A., Oubelaid, A., Bajaj, M., Tuka, M. B., & Kara, K. (2024). Lyapunov-based neural network model predictive control using metaheuristic optimization approach. *Scientific Reports*, *14*(1), 18760. https://doi.org/10.1038/s41598-024-69365-9

Tawade, P., & Mastrangeli, M. (2024). Integrated electrochemical and optical biosensing in organs-on-chip. *ChemBioChem*, *25*(3), e202300560. https://doi.org/10.1002/cbic.202300560

Tendulkar, M., Tendulkar, R., Dhanda, P. S., Yadav, A., Jain, M., & Kaushik, P. (2024). Clinical potential of sensory neurites in the heart and their role in decision-making. *Frontiers in Neuroscience*, *17*, 1308232. https://doi.org/10.3389/fnins.2023.1308232

Trunov, K., Kraiushkin, V., Zenkevich, A., & Khanas, A. (2025). Implementation of an artificial spiking neuron with photoreceptor functionality using gas discharge tubes. *Journal of Vacuum Science & Technology A*, *43*(3), 033002. https://doi.org/10.1116/6.0004433

Wang, S., Wu, M., Liu, W., Liu, J., Tian, Y., & Xiao, K. (2024). Dopamine detection and integration in neuromorphic devices for applications in artificial intelligence. *Device*, *2*(2), 100284. https://doi.org/10.1016/j.device.2024.100284

Wells, S. A., Morris, P. G., Taylor, J. D., & Nogaret, A. (2025). Estimation of ionic currents and compensation mechanisms from recursive piecewise assimilation of electrophysiological data. *Frontiers in Computational Neuroscience*, *19*, 1458878. https://doi.org/10.3389/fncom.2025.1458878

Yousuf, M., Rochet, J. C., Singh, P., & Hussain, M. M. (2025). Advancing brain organoid electrophysiology: Minimally invasive technologies for comprehensive characterization. *Advanced Materials Technologies*, *10*(7), 2401585. https://doi.org/10.1002/admt.202401585